Journal of Materials Chemistry C

Accepted Manuscript

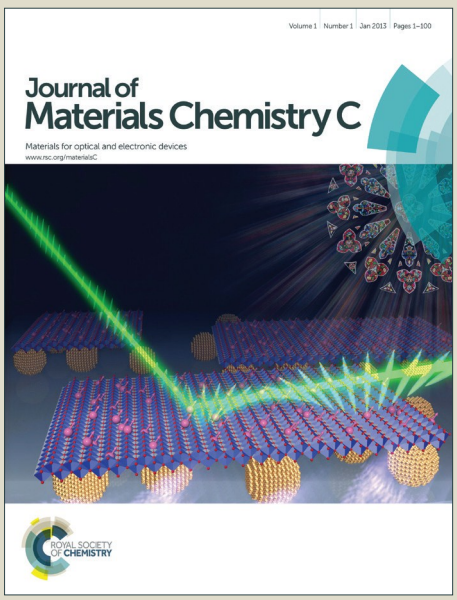

ROYAL SOCIETY OF CHEMISTRY

www.rsc.org/materialsC

Journal of

Materials Chemistry A

RSCPublishing

ARTICLE

Smectogenic Liquid Crystals and Nanoparticles: An Approach for Potential Application in Photovoltaics.

Cite this: DOI: 10.1039/x0xx00000x

Ariel Meneses-Franco [a], Andrés E. Fierro-Armijo [a], Patricio N. Romero-Hasler [a], L.G. Salamanca-Riba [b], L.J. Martínez-Miranda [b] and Eduardo A. Soto-Bustamante [a].

Received 00th January 2015,
Accepted 00th January 2015

DOI: 10.1039/x0xx00000x

www.rsc.org/

We synthetized monomeric liquid crystals M8R6 and I8R6, and nanoparticles of TiO_2, to form a nanocomposite, which was characterized by polarized optical microscopy (POM), DSC and structurally with both wide angle X-ray diffraction and by X-ray scattering using the planar geometry. The transition temperatures for the nanocomposites did not vary greatly with the concentration of TiO_2. The alignment quality increases as the concentration of TiO_2 increases from 7 to 30% wt as can be observed with the polarized microscopy and confirmed by the results of the X-ray scattering experiment. The alignment was not as good for I8R6, since in this case the liquid crystals attach to the nanoparticle just through the hydrogen bonding of the hydroxyl group in the aromatic cores. In the case of M6R8 an additional electrostatic interaction is present through the methacrylic groups which enhance the alignment. Although M6R8 shows better optical alignment, I6R8 presents a higher conductivity. This is because of the higher electron delocalization in the aromatic cores, where the nanoparticles are linked.

1. INTRODUCTION

A nanocomposite is a binary combination of at least one (in)organic or polymeric material mixed with nano-sized domains of a solid[1], which have attracted great interest and have been widely explored recently.[2-4] They can show improvements in mechanical,[5] optical,[6] magnetic,[7] electrical[8] and optoelectronic[9] properties of the original arrays. Some examples are ceramic semiconductor nanocrystals incorporated into polymer matrices.[10] Another example is the integrated capacitor used in the development of flexible electronics such as the development of display screens, circuit boards, or e-papers.[11] To reach these useful properties in many applications, it is very important to be able to disperse the nanocrystals homogeneously in the polymer matrix.[12, 13]

Interesting applications for nanocomposites are related with energy-saving devices, since we can combine dyes, liquid crystalline monomers or polymers as a well as titanium dioxide nanoparticles to prepare organic-inorganic photovoltaic cells.[14] It is well known that the Photo-voltaic (PV) effect is a simple technology, environmentally friendly and a non-pollutant energy source.[15] However, it is still an expensive renewable technology. Third generation solar cells technology considers triple junction and nanotechnology, which are all showing promising efficient cells at lower cost.[16, 17] The study of dye-sensitized nanocrystalline metal oxide solar cells has grown considerably in recent years from both a fundamental and an applied perspective.

LC's have high charge mobility compared to most organics materials due to the existence of the mesophase[18, 19]. They have been investigated for possible use of them in electron or hole conductors.[20] Work on dyes combined with LCs shows that it is possible to achieve one third increase in light emission due to the parallel aligned dye when compared with the isotropic mixtures.[21] In the mechanism for PV production the hole or the electron transporting material absorbs the light radiation, a mechanism which is enhanced when one of these materials possesses a higher electron affinity than the other.[19, 22, 23] Nanoparticles form rows within LCs[24] which turns into a path for electron and/or hole transfer between electrodes.

[a] Department of Organic Chemistry and Physical Chemistry, Faculty of Chemical and Pharmaceutical Sciences, University of Chile, Sergio Livingstone 1007, Independencia, Santiago, Chile.

[b] University of Maryland, Department of Material Science and Engineering and Energy Research Center, College Park, MD 20742-2115, United States..

We investigated the role of the ordering in the transfer of charges in the NpZnO-8CB liquid crystal system changing the concentration of ZnO in 8CB from 1.18 to 40% wt.[14] We found an improvement in the alignment of the liquid crystal with increasing weight percentage of Np, up to a concentration of 30% wt, with an increase in the current generated by the system by three orders of magnitude. The current depends both on the concentration of the nanoparticles and the order in the LC acquired as result of the interaction with the nanoparticles. We also found that for nanorods, this concentration was 35% wt.[25] More recently, we have found that the nanoparticles and the liquid crystals in the vicinity of the nanoparticles form a short range structure that still maintains a smectic order.[26]

On the other hand, we have been working in developing non-centrosymmetric materials that exhibit LC properties, being able to control antiferro-[27-33] and ferroelectricity[34] just by the proper choice of the organic structure.[35] These non-centrosymmetric systems and the main properties which affect the phenomena are already described.[36, 37]

In this work, we investigate two monomers to compare the polymerizable one with one that does not form a polymer. A polymer in photovoltaics has mechanical integrity compared with the monomeric compounds. This property gives better processability when compared with inorganic materials. On the other hand a liquid crystal is a more ordered system as compared with state of the art amorphous polymer

2. EXPERIMENTAL PART:

All reactive and solvents are of commercial grade and Pro Analysis, obtained from Merck Co and Aldrich. The synthesis of the titanium dioxide nanoparticles (henceforth called TONp) was carried out using two different methodologies. Method 1 (TONp-1) is a modification of $BaTiO_3$Np synthesis.[38] The second one (TONp-2) is a modified method of synthesis of Zinc oxide Np.[39] Both methods shown in Figure 1 can be summarized as follows:

Method 1 (TONp-1): A two neck rounded bottom flask containing 25 ml of isopropyl alcohol (IPA) was heated at 40 ºC with constant agitation and 27 ml of titanium tetraisopropoxide (TTPI) was added. When some vapour is exhausted 19 ml of glacial acetic acid is added. The temperature is raised to 60 ºC, maintaining the agitation for 30 min. Finally the temperature is slowly increased to 90 ºC and after a couple of minutes, allowed to cool to room temperature. The solution is always maintained with constant and vigorous agitation. The reaction mixture is dried for 12 hours at 150 ºC. The dried gel is milled with a mortar and the residue is heated in an oven at 500 ºC for one hour. 100 mg of the obtained nanopowder was suspended in 10 ml of DMF in an ultrasound bath for 6 hours. After this time, the suspension is centrifuged at 3000 rpm for 5 minutes. The amount of TONp in the supernatant is evaluated by weighting the remaining TONp obtained after drying a specific volume of this supernatant.

Method 2 (TONp-2): In a round bottom flask 10 ml of titanium tetraisopropoxide (TTIP) was dissolved with 40 ml of isopropyl alcohol (IPA) and gently heated to 40 ºC for 30 min. After this time, this solution was added dropwise to a 50 ml aqueous solution of NH_4OH 1M maintained at 60 ºC, under vigorous stirring. The reaction mixture is heated and refluxed for 1 hr. The obtained suspension was centrifuged at 5000 rpm for 10 min and washed several times with deionized water until neutral pH is achieved, and finally resuspended in ethanol.

Figure 1. Scheme showing the procedure for the synthesis of the nanoparticles: left side TONp-1, right side; TONp-2.

The samples were observed by transmission electron microscopy (TEM) using a Zeiss microscope, model EM-109 in copper grids, which were covered with FORMAVAN® as support, for aqueous samples and carbon in the case of organic samples to determine the size distribution of the nanoparticles. The TEM images were analysed with software Axio Vision Rel. 4.8 image processor.

High Resolution Transmission Electron Microscopy characterization (HR-TEM) was performed using a JEOL 2100 F field emission TEM operated at 200 KV. The microscope has a spherical aberration coefficient of 0.5 mm and chromatic aberration of 1.1 mm. We obtained electron diffraction patterns, medium and high resolution lattice images from many particles for characterization. The TEM samples were prepared by delivering a drop of solution containing the particles on a carbon coated TEM grid and allowing it to dry.

Measurements of X-ray diffraction in nanopowder samples were performed in a D5000 SIEMENS diffractometer in concentric rings DK plate 5 cm, using CuK_α radiation (1.5418 Å).

The IR spectra of nanopowders were obtained in a FT-IR Brüker IFS28 spectrophotometer operated by OPUS software in the transmission mode; the samples were dispersed in KBr spectroscopy grade powder.

The material to prepare the organic composites M30 and I30

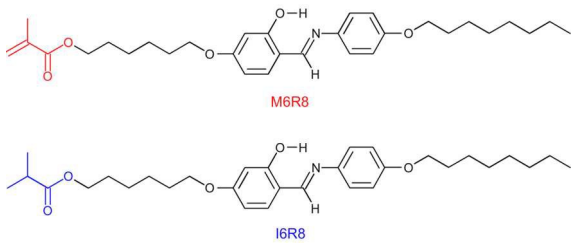

Figure 2. Structures of the monomers studied. M6R8 has a polymerizable methacrylate group while I6R8 has a non-polymerizable iso-propylester moiety.

corresponds to the monomers M6R8 and I6R8 respectively (see Figure 2). The preparation of M6R8 was carried out using a convergent synthetic pathway already described.[40, 41] Monomer I6R8 is already described in detail elsewhere.[42] A summarized description follows.

Isobutyryl chloride, prepared from isobutyric acid and thionyl chloride, was reacted with 6-chlorohexan-1-ol to obtain 6-chlorohexyl isobutyrate (I6Cl). This ester was submitted to a halogen exchange with iodine using the Finkelstein reaction.[43] The prepared 6-Iodohexyl isobutyrate (I6I) was reacted with 2,4-dihydroxybenzaldehyde to obtain the 6-(4-formyl-3-hydroxyphenoxy) hexyl isobutyrate (I6). Finally a condensation with octyloxyaniline yield the desired final product (E)-6-(3-hydroxy-4-(((4-(octyloxy)phenyl)imino]methyl)phenoxy)hexyli sobutyrate (I6R8).

$C_{31}H_{45}NO_5$ (I6R8) ^{1}H-NMR ($CDCl_3$) δ ppm: 13.86 (s, 1H, OH-Ar); 8.43 (s,1H, -CH=N); 7.16 (d, 1H, βH-Ar-CH=N); 7.15 (d, 2H, βH-Ar-N=CH-); 6.85 (d, 2H, βH-Ar-O); 6.40 (s, 1H, βH-Ar-OH); 6.39 (d, 1H, βH-Ar-OR); 4.01 (t, 2H, CH_2-OOC-); 3.93-3.90 (t, 4H, CH_2-O-); 2.47 (m, 1H, -CH-COO-); 1.72 (m, 4H, βCH_2-O-); 1.62 (m, 2H, βCH_2-OOC-); 1.39-1.20 (m, 14H; -CH_2-); 1.09 (d, 6H, δCH_3-COO-); 0.82 (t; 3H, -CH_3). Elemental analysis calculated for the I6R8, C: 72.77%, H 8.86%, N 2.74%, O 15.63% found C: 72.78%, H 9.04%, N 2.95%, O 15.23%. Analysis of mass calc exact mass molecular weight 511, and found m/z+ 511.71.

To manufacture the nanocomposites, an exact amount of liquid-crystalline matrix, around 150 mg was dissolved in DCM. Then the required amounts of both suspensions of nanoparticles TONp-1 and TONp-2, were measured to obtain the desired final weight percentage of the nanoparticles. The solutions were submitted to ultrasound for about 30 minutes and dried under vacuum at 80 ºC, for a quick but gentle solvent evaporation.

The phase transition temperatures for the investigated samples were determined using a differential thermal analyzer (Mettler, FP90 DTA). The DTA was calibrated using three different standards: benzophenone (ME18870) m.p. 47.9 ± 0.2 ºC; benzoic acid (ME18555) 12.3 ± 0.2C and caffeine (ME18872) 236.0 ± 0.3 C. As control we use Indium (156.6 ºC) and a ramp rate of 4 ºC/min (±0.1K).

The POM (polarized optical microscopy) characterization was taken in a polarizing microscope (Leica, DLMP), equipped with a heating stage (Instec HCS-402). The microscope was used for temperature dependent investigations of liquid crystal textures. A video camera (Nikon DXM1200) installed on the polarizing microscope allowed for real time image capture, via coupling with a Nikon video capture card. The samples were studied in commercial cells (Instec LC-4) with planar antiparallel alignment induction layer. A cell gap of 6.8µm and 0.25mm^2 square ITO electrodes.

The current vs voltage (I-V) curves were obtained using a 5mhz/30Vpp triangular wave (arbitrary waveform generator TTi TG1010), while the current was registered with a multimeter in series to the cell (Agilent HP34401A). The monomers and nanocomposites were used in the Instec cells aforementioned.

The X-ray experiments to study the LC nanocomposites as powder were performed using a Rigaku rotating anode with a Cu 1.54 Å source, and a bent graphite monochromator with a resolution of $\Delta q = 0.012 q_0$ Å^{-1}, operating at 50 kV and 100 mA (a,b). The rotating anode allows a broad working angle, depending on the monochromator and the slits of the apparatus from 1.5º to 70º. The incoming beam was parallel to the surface of the substrate. This scan is not strictly a grazing incidence scan, although its geometry is the same.[44] The samples M30

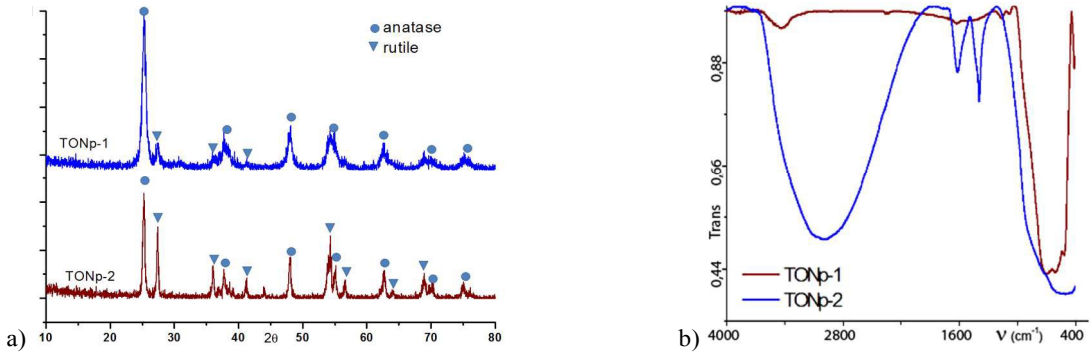

Figure 3. TONp-1 and TONp-2; a) powder X-ray diffraction and b) FT-IR spectra.

and I30 were collected in a glass substrate without any previous treatment, and properly centered such as they are cutting the X-ray beam. A background was taken only with the substrate, and was subtracted before the analysis was performed.

3. RESULTS

TiO_2 synthetized through method 1 (TONp-1) shows a structural dependence with calcination temperature. At 500 ºC, a nanostructure anatase is obtained, whereas at 800˚C, one obtains the rutile structure with a size between 50 and 60 nanometers. TiO_2 Synthetized using method 2 (TONp-2) shows a mixture of both the rutile and the anatase crystal structures. These results were obtained using wide angle X-rays in the nanopowders (see Figure 3.a).

In the FT-IR spectra shown in Figure 3.b for the precursors of TONp-1 there is a signature typical of organometallic complexes, which implies that the structure is probably $Ti_aO_b(OiPr)_c(OAc)_d$.[45] When it is heated to 500 ºC the precursor decomposes and generates a signal typical of TiO_2. A wide signal can be observed around 1450 cm^{-1}, as well as lines that correspond to CO_3^{2-} (1650 and 1350 cm^{-1}). The product obtained when the sample is prepared at 800 ºC does not exhibit crystalline structure. Anatase is capable of adsorbing a greater amount of water and CO_2 at the surface, due to electrostatic interactions. This explains its capacity to generate OH moieties and CO_3^{2-}.[46]

The precursor for TONp-2 corresponds to H_2TiO_3 or $TiO(OH)_2$. When the sample is heated up, it decomposes to form TiO_2. This process occurs through dehydration that in general produces a large quantity of OH groups at the surface, as observed in the IR-spectra. A characteristic O-H stretching signal in the FTIR spectrum can be seen only for the TONp-2. This can be logically explained due to the method of synthesis for these nanoparticles. In an aqueous precipitation, without calcination, the presence of hydroxyl groups in the nanoparticles' surface is natural. This group has an effect on how the nanoparticles interact inside the liquid crystalline matrix. This hydroxyl groups affect the interaction with the polar groups present in the aromatic centers, and the methacrylic group of the liquid crystalline matrix as we show.

Table 1: Thermodynamic data of investigated samples.

	Heating				Cooling	
Comp.	MP (ºC)	ΔH_1 (J/g)	CP (ºC)	ΔH_2 (J/g)	EP (ºC)	ΔH_2 (J/g)
I	62.7	48.1	98.3	7.93	98.1	-10.6
I 7	60.9	45.2	98.1	9.38	97.1	-9.33
I 15	62.7	31.9	97.9	5.89	96.6	-4.76
I 30	61.8	29.4	97.9	2.74	97.3	-4.32
M	56.2	28.7	97.7	6.25	97.2	-7.28
M 7	55.4	35.5	97.5	3.48	96.9	-3.81
M 15	55.6	61.1	97.6	8.04	97.0	-8.45
M 30	55.1	45.1	97.1	5.96	96.5	-6.5

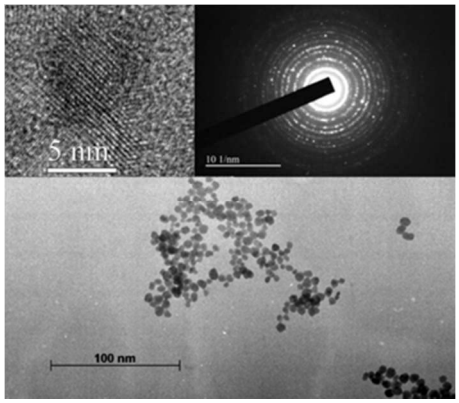

Figure 4. TEM images for TiO_2. Upper images: HRTEM image of a single particle and an electron diffraction pattern for the particles. Lower image: A low resolution TEM showing the relative uniformity of the particles.

A particle size of 3-5 nm of diameter was obtained for the TONp-1, when the calcination temperature was 500 ºC. This product was aggregated in a fibrillar fashion, and was difficult to re-suspend. For the TONp-2, the particle size obtained was quite homogeneous, at around 5 nm. Measurements carried out on nanocomposite samples using X-ray scattering in the planar geometry yields a size of 4±1 nm. The TONp-2 particles were far less aggregated which made them easier to be re-suspended. Figure 4 shows a HR-TEM of a 5nm particle from TONp-1 in the left top side of the figure. Beside it is a diffraction pattern which shows numerous rings because the beam of electrons included a large number of particles with different orientations. It shows rings of spots corresponding to the random orientation of the nanoparticles. The bottom picture is a low resolution image of the TONp-1 showing the size uniformity of the particles.

It has been described previously that the monomers form mono-layered SmA and SmC phases.[47] Table 1 summarizes the phase transitions for all compounds and nanocomposites studied by means of DTA. The nanoparticles do not seriously modify the liquid crystalline properties of original monomeric compounds, as can be seen in the table. This also agrees with the X-ray scattering results for the 30% nanocomposite sample of M6R8 shown in Figure 5.

Interestingly, there is a destabilization of the mesophases for the I-series as soon as the TiO_2 concentration increases, as evidenced in the decrease in the enthalpy values. For the M-series, the situation changes and the nanoparticles' addition provoke an increase in enthalpy until the M15 nanocomposite.
We believe that the nanoparticles locate themselves at the layer interface where the methacrylic groups are present. The decrease of the enthalpy and therefore the mesophase stability can be understood as a distribution of more nanoparticles at the

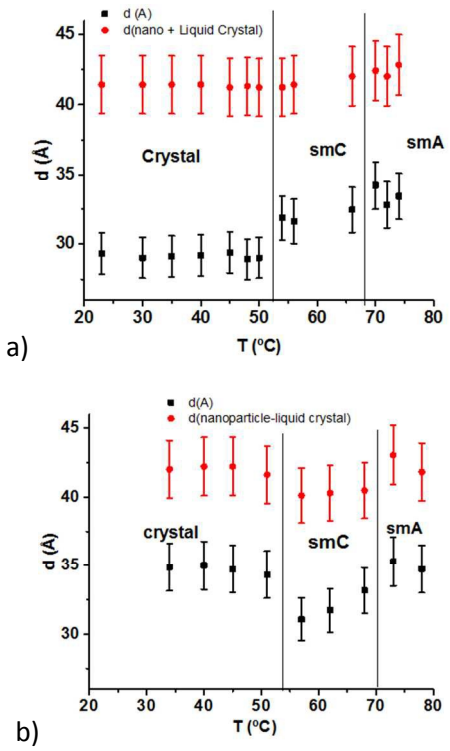

Figure 5. Interlayer distances d for liquid crystalline nanocomposites possessing 30% wt. of TONp a) M6R8 (M30) and b) I6R8 (I30).

aromatic cores, since no more places is allowed at the layer interface.

The molecular length L of monomeric compounds was calculated using MOPAC93 Molecular Approximation Software. Here, L equals the length of the molecule, in the stretched conformation, between the last carbon atom in the aliphatic flying tail and the first ethylenic carbon atom of the methacrylic group. The calculus was carried out for M6R8 since just a minimal variation in length for the carbon double bond must be considered for I6R8. Then, the theoretical length L for I6R8 and M6R8 amounts 32.04 Å for both compounds.

A correlation between the quality of alignment of the mesophases and the nanoparticle concentration can be seen from the POM investigations, especially for the composites using M6R8 as matrix (see Figure 6).

For this study, the cells have a polyimide antiparallel planar alignment layer. The monomeric compounds tend to align homeotropically in untreated glass. The alignment quality of these nanocomposites improves when the nanoparticle concentration increases from 7 to 30% wt. This same trend was also observed in the case of ZnO in 8CB.[14, 25] This can be easily distinguished in the texture analysis taken at 70 ºC for each sample, as seen in Figure 6.

This unusual behaviour for the improved alignments of M6R8 compared with I6R8 nanocomposites samples motivated us to perform more detailed experiments with the planar X-ray scattering geometry. We concentrate our efforts in comparing M30 against I30 nanocomposites exhibiting this high alignment difference (see Figure 6.a M30 and 6.b I30). Although not shown here, M15 and M30 exhibit a significantly better extinction ratio by rotating the angle of the cell between crossed polarizers.

X-ray measurements in planar geometry for all the 30% weight nanocomposites indicate the existence of normal smectic C and A phases. The molecular spacing was obtained by analysing the X-ray scattering scans with a Gaussian curve statistic and obtaining the best fits. This fits gives a d-spacing, shown in Figure 5, which agrees within error with the calculated theoretical length using MPOAC93 software. The transitions from crystal to SmC agree with the DSC measurements for the M30 and the I30 sample. The SmC – SmA transition lies around 70˚C for both M30 and I30. These results showed a higher d-peak for both samples at about 42 Å (see Figure 5). This peak is associated to the combination of the nanoparticle and the liquid crystal matrix that holds the nanoparticles in place. This demonstrate the formation of a composite instead of a simple heterogeneous mixture of two components. The intensity of this peak increases by at least one order of magnitude when the crystal phase transition point is reached around 52 ˚C. The fact that it does not disappear shows the interaction of the nanoparticles and the liquid crystal.

A possible proof of the disorder seen in the I30 nanocomposite versus the M30 nanocomposite can be observed with the X-rays when the crystal phase is achieved. The liquid crystalline phase that is “frozen” in the solid state corresponds to the SmC phase

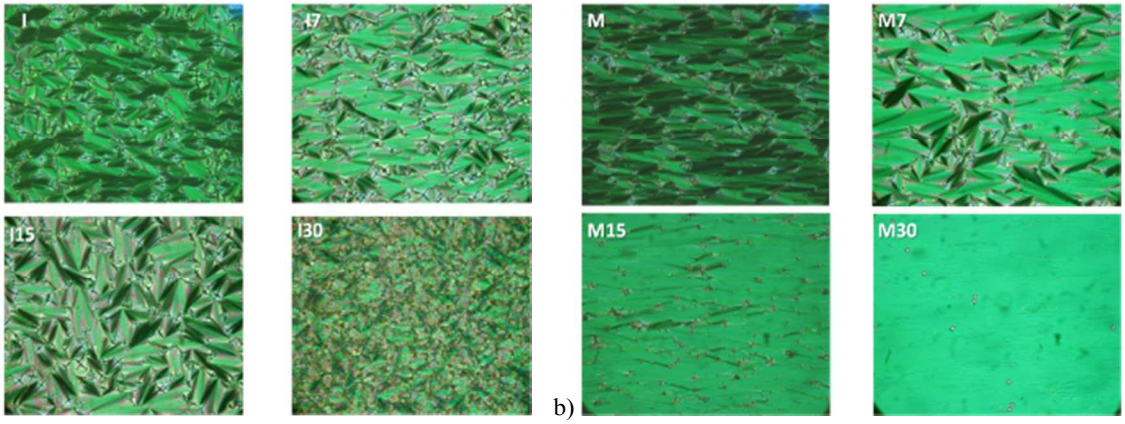

Figure 6. Polarizing Microscope images for a) M6R8 and b) I6R8 nanocomposites at different nanoparticles concentration ranging from 0 to 30% wt.

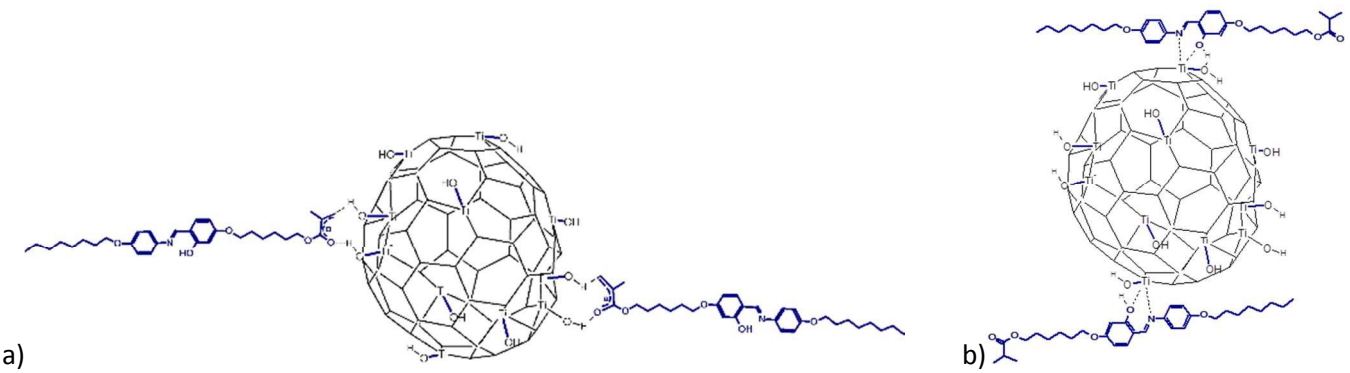

Figure 7. Possible ways the monomer attaches to the TiO_2 nanoparticle. a) Through the methacrylate group only possible in M6R8 or b) through the Schiff base as in I8R6 and M6R8.

for the M30 sample and the SmA phase for the I30 sample (see Figure 5). The SmA phase is a higher temperature phase and hence has more thermal disorder associated with it. The liquid crystal aligns with the nanoparticle in the I30 phase in a planar arrangement, and creates a defect structure around the nanoparticle which propagates into the sample[26, 48]. The more disordered phase results in a variation in the I30 liquid crystal phase (see Figure 5.b) of the high d-peak if compared with the M30 liquid crystal phase, where the high d-peak remains more or less constant (see Figure 5.a).

We believe there are two kinds of interaction capable of explaining the experimental results. The only significant structural difference between the two monomers M6R8 and I6R8 included in the two nanocomposites M30 and I30 is the presence (M6R8) or absence (I6R8) of a double bond at the end of one of the aliphatic tails. Therefore, two possible interactions between the liquid crystal and the nanoparticle surface can be established for M6R8: via the methacrylate group and the Schiff base group (see Figure 7). The methacrylic group is rich in electron density due to the double bond conjugation. In this interaction, the molecular steric hindrance is smaller than through the Schiff base: the whole molecule is free to rotate far away from the nanoparticle surface. It is even possible to argue a 1,4-addition between the methacrylate group and the free OH group in the surface of the Np. Other authors have argued about the possibility of Michael-type addition mechanism in the presence of basic and/or nucleophilic initiators, for methacrylic and acrylic compounds.[49] This is due to the fact that the nucleophilicity of the OH group bonded to titanium is higher compared with the OH hanging from C atoms. In the case of I6R8 the only interaction is through the Schiff base group. Hydrogen bridges through the Schiff Base group are responsible for the nanoparticle-liquid crystal interaction for both materials. This interaction causes a high repulsion from the hydrophobic aliphatic tails with the nanoparticle surface which is rich in hydroxyl groups. A high molecular steric hindrance must be expected through the Schiff base interaction due to the rigidity of the aromatic core, and proximity of the whole molecule with the nanoparticle surface (see Figure 7.b).

Figure 8.a show the results of the current as a function of temperature for both composites with and without nanoparticles. The data for each temperature were calculated as the average current maximum when a triangular electric Bias of 0.1 mHz of 30 Vpp is applied. The curves clearly show a difference between both samples, being ten times larger in the case of the I series. This confirms our previous assumption, that the nanoparticles are attached preferentially to the aromatic rings in case of I series, since no methacrylic groups are present in these molecules. Samples of M series show very low conductivities which must be understood as a preferential nanoparticle interaction with the methacrylic groups.

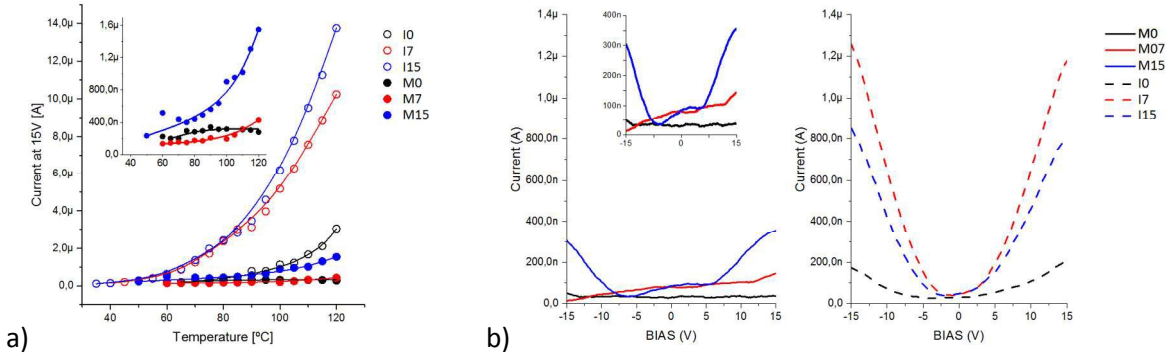

Figure 8. a) I-T curves for the investigated I6R8 liquid crystalline monomers and its nanocomposites at 15 V. The inset shows a magnification of the obtained values for M composites; b) I vs V characteristics of both the I and M series at 60 ºC.

Interestingly, samples of the methacrylic compound also show a degree of uncontrolled polymerization which in this case also disorders to some extent the nanocomposites which have been formed. Figure 8.b shows the V-I curves for samples at 60 ºC. The curves are rectifying even though they show a relatively small current for the M series. This is due to the interaction with the methacrylic group which is polar in nature.

The 30% wt of TiO_2 is the most ordered for both the M and the I samples. The results from the current as a function of temperature for these samples show that in addition to having the sample ordered, it must be ordered such that the delocalized electrons at the aromatic cores faces the nanoparticle. The additional electrostatic interaction through the methacrylic groups in M6R8 enhances the alignment. Although M6R8 shows better optical alignment, I6R8 presents a higher conductivity. This is because of the higher electron delocalization in the aromatic cores, where the nanoparticles are strictly linked.

Conclusions

We have prepared two monomers to compare the polymerizable one with one that does not form a polymer. We added two types of TiO_2 nanoparticles to investigate which one produces the better nanocomposites. The best nanocomposites are obtained with nanoparticle TONp-2 which possesses a mixture of rutile and anatase.

Nanocomposites showed two different behaviours. There is a better optical alignment achieved with 30% of nanoparticles in the methacrylic M6R8 monomer. On the other hand, a better electrical pattern is obtained in the samples with no methacrylic group, where the only interaction with the nanoparticle is through the Schiff base group.

The transition temperature of both M6R8 and I6R8 does not vary significantly as the nanoparticle is added. However, the enthalpy values argue for a destabilization of the mesophases in the I-series. For the M-series the nanoparticles addition provoke a stabilization of the smectic phases while the nanoparticle increases its concentration until a certain point. There is evidence that the nanoparticles locate also at the aromatic cores beyond this point, since no more place is allowed at the layer interface.

I-V curves taken at definite temperatures show increases of the current for the I-series. The same values for the M-series show a comparable pattern which is significantly lower, at least one order of magnitude. This reflects the association with the nanoparticle. The association of the nanoparticle with the methacrylic group results in a polar separation of the charges that does not produce a current. The association of the nanoparticle with the Schiff bases produces a current through the delocalized electrons.

Acknowledgements

A. Meneses-Franco and P. Romero-Hasler acknowledge Conicyt scholarship for doctoral studies. E. A. Soto-Bustamante thanks Fondecyt Project 1130187. L.J. Martínez-Miranda thanks a Fulbright Specialist Program Fellowship and NSF-OISE-1157589.

References

1. S. C. Tjong, *Materials Science and Engineering: R: Reports*, 2006, **53**, 73-197.
2. J. L. Dewald, W. T. Wondmagegn, A. V. Ellis and S. A. Curran, *Synthetic Metals*, 2005, **155**, 39-44.
3. S. Komarneni and J. C. Parker, Nanophase and Nanocomposite Materials, Materials Research Society, Pittsburgh, 1993, pp. 246.
4. C. K. Chung, P. K. Fung, Y. Z. Hong, M. S. Ju, C. C. K. Lin and T. C. Wu, *Sensors and Actuators B: Chemical*, 2006, **117**, 367-375.
5. G. Carotenuto, B. Martorana, G. LaPeruta, A. Longo, P. Perlo and L. Nicolais, *Sensors and Actuators A: Physical*, 2006, **132**, 541-546.
6. J. Li and J. Z. Zhang, *Coordination Chemistry Reviews*, 2009, **253**, 3015-3041.
7. J. Jiang, L. Li and M. Zhu, *Reactive and Functional Polymers*, 2008, **68**, 57-62.
8. M. G. Kanatzidis, T. J. Marks, H. O. Marcy, W. J. McCarthy and C. R. Kannewurf, *Solid State Communications*, 1988, **65**, 1333-1337.
9. F. Piret, C. Bouvy, W. Marine and B. L. Su, *Chemical Physics Letters*, 2007, **441**, 83-87.
10. S. Tkaczyk, M. Galceran, S. Kret, M. C. Pujol, M. Aguiló, F. Díaz, A. H. Reshak and I. V. Kityk, *Acta Materialia*, 2008, **56**, 5677-5684.
11. J. P. F. Lagerwall, R. Dabrowski and G. Scalia, *Journal of Non-Crystalline Solids*, 2007, **353**, 4411-4417.
12. M.-A. Kakimoto, A. Takahashi, T.-a. Tsurumi, J. Hao, L. Li, R. Kikuchi, T. Miwa, T. Oono and S. Yamada, *Materials Science and Engineering: B*, 2006, **132**, 74-78.
13. J. Móczó and B. Pukánszky, *Journal of Industrial and Engineering Chemistry*, 2008, **14**, 535-563.
14. L. J. Martínez-Miranda, K. M. Traister, I. Meléndez-Rodríguez and L. Salamanca-Riba, *Applied Physics Letters*, 2010, **97**, 223301.
15. L. El Chaar, L. A. lamont and N. El Zein, *Renewable and Sustainable Energy Reviews*, 2011, **15**, 2165-2175.
16. B. R. Saunders and M. L. Turner, *Advances in Colloid and Interface Science*, 2008, **138**, 1-23.
17. N. G. Park, J. van de Lagemaat and A. J. Frank, *The Journal of Physical Chemistry B*, 2000, **104**, 8989-8994.
18. J. Nelson, *Science*, 2001, **293**, 1059-1060.
19. M. T. Lloyd, J. E. Anthony and G. G. Malliaras, *Mater. Today*, 2007, **10**, 34-41.
20. R. J. Bushby and O. R. Lozman, *Curr. Opin. Solid State Mater. Sci.*, 2002, **6**, 569-578.
21. P. P. C. Verbunt, A. Kaiser, K. Hermans, C. W. M. Bastiaansen, D. J. Broer and M. G. Debije, *Adv. Funct. Mater.*, 2009, **19**, 2714-2719.
22. L. J. A. Koster, V. D. Mihailetchi and P. W. M. Blom, *Applied Physics Letters*, 2006, **88**, 093511.
23. A. Moliton and J.-M. Nunzi, *Polymer International*, 2006, **55**, 583-600.
24. J.-C. Loudet, P. Barois and P. Poulin, *Nature*, 2000, **407**, 611-613.
25. J. Branch, R. Thompson, J. W. Taylor, L. Salamanca-Riba and L. J. Martínez-Miranda, *Journal of Applied Physics*, 2014, **115**, 164313.
26. Taylor, Ph. D. Thesis, University of Maryland, 2013.
27. E. A. Soto-Bustamante, S. V. Yablonskii, B. I. Ostrovskii, L. A. Beresnev, L. M. Blinov and W. Haase, *Liq. Cryst.*, 1996, **21**, 829-839.
28. E. A. Soto-Bustamante, S. V. Yablonskii, B. I. Ostrovskii, L. A. Beresnev, L. M. Blinov and W. Haase, *Chem. Phys. Lett.*, 1996, **260**, 447-452.
29. D. R. Link, N. A. Clark, B. I. Ostrovskii and E. A. Soto Bustamante, *Physical Review E*, 2000, **61**, R37-R40.

30. E. A. Soto-Bustamante, R. Werner, T. Weyrauch, P. A. Navarrete-Encina and W. Haase, *Chem. Phys. Lett.*, 2000, **322**, 45-50.
31. E. A. Soto Bustamante, P. A. Navarrete Encina, T. Weyrauch and R. Werner, *Ferroelectrics*, 2000, **243**, 125-135.
32. S. V. Yablonskii, T. Weyrauch, S. Grossmann, R. Werner, E. A. Sotobustamante, W. Haase, S. G. Yudin and L. M. Blinov, *Ferroelectrics*, 2000, **247**, 343-354.
33. S. V. Yablonski, Y. P. Pisarevski, S. G. Yudin and E. A. Soto-Bustamante, *J. Soc. Electron. Mater. Eng*, 2005, **14**, 119-120.
34. S. V. Yablonskii, E. A. Soto-Bustamante, R. O. Vergara-Toloza and W. Haase, *Advanced Materials*, 2004, **16**, 1936-1940.
35. E. A. Soto-Bustamante, R. O. Vergara-Toloza and W. Haase, *Journal of Materials Chemistry*, 2012, **22**, 17753-17758.
36. E. A. Soto-Bustamante, R. O. Vergara-Toloza and C. M. González-Henríquez, *Chemical Physics Letters*, 2012, **544**, 22-27.
37. C. M. González-Henríquez, E. A. Soto-Bustamante and W. Haase, *Chem. Phys. Lett.*, 2012, **545**, 29-34.
38. A. Meneses-Franco, V. H. Trujillo-Rojo and E. A. Soto-Bustamante, *Phase Transitions*, 2010, **83**, 1037-1047.
39. M. Y. Ge, H. P. Wu, L. Niu, J. F. Liu, S. Y. Chen, P. Y. Shen, Y. W. Zeng, Y. W. Wang, G. Q. Zhang and J. Z. Jiang, *Journal of Crystal Growth*, 2007, **305**, 162-166.
40. E. A. Soto-Bustamante, Y. G. Galyametdinov, K. Griesar, E. Schuhmacher and W. Haase, *Macromolecular Chemistry and Physics*, 1998, **199**, 1337-1342.
41. E. A. Soto-Bustamante and W. Haase, *Liquid Crystals*, 1997, **23**, 603-612.
42. R. O. Vergara-Toloza, Universidad de Chile, 2006.
43. H. Finkelstein, *Berichte der deutschen chemischen Gesellschaft*, 1910, **43**, 1528-1532.
44. L. J. Martínez-Miranda and L. K. Kurihara, *Journal of Applied Physics*, 2009, **105**, 084305.
45. F. X. Perrin, V. Nguyen and J. L. Vernet, *Journal of Sol-Gel Science and Technology*, 2003, **28**, 205-215.
46. U. Diebold, *Surface Science Reports*, 2003, **48**, 53-229.
47. E. A. Soto-Bustamante, D. Saldaño-Hurtado, R. O. Vergara-Toloza, P. A. Navarrete-Encina and M. A. Athanassopoulou, *Liq. Cryst.*, 2003, **30**, 17-22.
48. J. W. Taylor, L. K. Kurihara and L. J. Martínez-Miranda, *Applied Physics Letters*, 2012, **100**, 173115.
49. B. D. Mather, K. Viswanathan, K. M. Miller and T. E. Long, *Progress in Polymer Science*, 2006, **31**, 487-531.